

## Triaxial shape coexistence and new aligned band in $^{178}\text{Os}$

Rajesh Kumar,<sup>1,\*</sup> I. M. Govil,<sup>1,†</sup> A. Dhal,<sup>2</sup> L. Chaturvedi,<sup>2,‡</sup> C. R. Praharaj,<sup>3</sup> A. K. Rath,<sup>4</sup> G. Kiran Kumar,<sup>5</sup> S. K. Basu,<sup>6</sup> A. Chakraborty,<sup>7</sup> Krishichayan,<sup>7</sup> S. Mukhopadhyay,<sup>7,‡</sup> N. S. Pattabiraman,<sup>7</sup> S. S. Ghugre,<sup>7</sup> and A. K. Sinha<sup>7</sup>

<sup>1</sup>*Department of Physics, Panjab University, Chandigarh-160014, India*

<sup>2</sup>*Department of Physics, Banaras Hindu University, Varanasi-220115, Uttar Pradesh, India*

<sup>3</sup>*Institute of Physics, Bhubaneswar-751005, India*

<sup>4</sup>*Department of Physics, Sambalpur University, Jyoti Vihar, Burla, Sambalpur-768019, Orissa, India*

<sup>5</sup>*Department of Physics, Maharaja Sayajirao University, Vadodara, Baroda 390002, India*

<sup>6</sup>*Variable Energy Cyclotron Center, Bidhan Nagar, Calcutta-700064, India*

<sup>7</sup>*UGC-DAE Consortium for Scientific Research, Calcutta Centre, Sector III LB-8, Bidhan Nagar, Kolkata-700098, India*

(Received 26 November 2008; revised manuscript received 14 August 2009; published 30 November 2009)

High spin states in  $^{178}\text{Os}$  were studied by means of  $^{165}\text{Ho}(^{20}\text{Ne},p6n)^{178}\text{Os}$  fusion evaporation reaction at a beam energy of 150 MeV, using a clover detector array. Several new transitions belonging to  $^{178}\text{Os}$  were placed in a level scheme and a new aligned rotational band was observed in addition to earlier known bands. Spin-parity assignments for most of the proposed levels were made using the deduced directional correlation orientation and polarization measurements for the de-exciting transitions. Experimental results are compared with the projected angular momentum deformed Hartree-Fock model calculations and cranked Woods-Saxon model calculations. This nucleus is predicted to be prolate deformed in the ground state but the  $\gamma$ -softness at higher excitation is revealed by the cranked Woods-Saxon model and the geometrical asymmetric model calculations.

DOI: [10.1103/PhysRevC.80.054319](https://doi.org/10.1103/PhysRevC.80.054319)

PACS number(s): 23.20.Lv, 21.10.Hw, 25.70.Hi, 27.70.+q

### I. INTRODUCTION

During the last two decades, studies of nuclei far from stability and at high spin have led to numerous discoveries such as shape coexistence, band crossing at high spins, dynamic effects, superdeformation, the importance of shell gaps at large deformations, and competition between prolate and oblate shapes. The Os nucleus belongs to the transitional region between well-deformed rare earth and spherical lead isotopes. The nuclei in this mass region are believed to be  $\gamma$ -soft to changes in deformation owing to the softness of nuclear potential and, consequently, may result in shape coexistence. Neutron Fermi levels in Os nuclei from  $A = 170$  to  $A = 186$  lie in the middle of the  $i_{13/2}$  orbitals, so that their shape tends to take an appreciable prolate deformation. Rotational bands of osmium isotopes display very interesting properties that vary with neutron number [1–4]. These have approximately constant quadrupole deformation  $\beta_2$  and varying hexadecapole deformation  $\beta_4$  [5]. Yrast bands of  $^{182,184,186}\text{Os}$  nuclei display a rather sudden and strong gain in aligned angular momentum at rotational frequencies of  $\hbar\omega = 0.26$  to  $0.30$  MeV [1,6]. Their interaction has been interpreted in terms of rotational alignment of an  $i_{13/2}$  quasineutron pair with fairly weak interaction between the crossing bands [7].  $^{176,178,180}\text{Os}$  nuclei, on the contrary, experience crossings with strong interactions characterized by an irregular but gradual increase in alignment [2,8].

Deformation susceptibility (softness) and triaxial shapes are also expected for Os nuclei, as they are located at the upper edge of the deformed region. In this region three high- $j$  shells lie close to the Fermi surface, that is, the  $i_{13/2}$  neutron and the  $h_{9/2}$  and  $h_{11/2}$  proton shells. A search for band crossings due to rotational alignment of quasiproton pairs requires an extension of rotational bands to large angular momenta. The  $^{178}\text{Os}$  nucleus has been studied by Dracoulis *et al.* [9] using the  $^{166}\text{Er}(^{16}\text{O},4n)^{178}\text{Os}$  reaction, by Kibedi *et al.* [10] using the  $\beta$  decay of  $^{178}\text{Ir}$ , and by Burde *et al.* [11] using the  $^{154}\text{Sm}(^{29}\text{Si},5n)^{178}\text{Os}$  reaction in different aspects. Dracoulis *et al.* have tentatively reported a  $\beta$ -band with the band head at 1167 keV ( $4^+$  state). They have also reported a few weak negative-parity bands, but no  $\gamma$ -band. Kibedi *et al.*, on the contrary, have reported a strong  $\gamma$ -band with the band head at 864 keV ( $2^+$  state) and, also, a  $\beta$ -band with the band head at 650 keV ( $0^+$  state). They have, however, reported only one weak negative-parity band, with the band head at 1302 keV ( $3^-$  state). Burde *et al.* [11] have reported an unusual, most likely superdeformed, band at 6956 keV ( $26^+$  state). It consists of seven regularly spaced transitions, 36 keV apart, which corresponds closely to the superdeformed band in  $^{152}\text{Dy}$  after  $A^{5/2}$  normalization. The presence of anomalies in osmium isotopes and the observation of an unusual rotational band in  $^{178}\text{Os}$  motivated us to investigate this nucleus further at high spin. Another motivating factor was to look for features associated with the collective rotation bands, for example, shape transition, band crossing, and proton alignment at higher excitation. In the present work, we observed several new  $\gamma$  transitions. We have also attempted to establish unambiguously the spin-parity of the already existing bands using linear polarization measurements and angular correlations. A new aligned band was observed in this nucleus for the first time.

\*Present address: Department of Physics, J.C. D.A.V. College Dasuya, Hoshiarpur, India.

†GGU (Central University), Bilaspur (Chhattisgarh), India.

‡Department of Physics, Mississippi State University, Mississippi State, MS 39762, USA.

## II. EXPERIMENTAL DETAILS AND DATA ANALYSIS

High spin states in the  $^{178}\text{Os}$  nucleus were populated using the  $^{165}\text{Ho}(^{20}\text{Ne}, p6n)^{178}\text{Os}$  fusion evaporation reaction at a beam energy of 150 MeV. A  $^{20}\text{Ne}$  beam was delivered from the variable-energy cyclotron (Variable Energy Cyclotron Centre [VECC], Calcutta). A self-supporting enriched  $^{165}\text{Ho}$  target  $\sim 4$  mg/cm<sup>2</sup> thick was used in the experiment. The  $\gamma$ -rays emitted from residual nuclei were observed using the Indian National Gamma Array (INGA), stationed at the VECC. For this experiment, the INGA comprised six Compton-suppressed clover detectors, two each at angles of 40°, 90°, and 125°, with respect to the beam direction. A total of about  $3 \times 10^8$  two- or higher-fold  $\gamma$ - $\gamma$  coincidence events were collected in the experiment. Efficiency and energy calibration were performed with the standard  $\gamma$ -ray  $^{152}\text{Eu}$  and  $^{133}\text{Ba}$  radioactive sources. After gain matching, coincidence events were sorted into symmetric and asymmetric (angle-dependent) matrices for detailed off-line analysis. Data were analyzed using both RADWARE [12] and IUCSORT [13] computer software packages.

A method based on observation of the direction correlation of  $\gamma$ -rays de-exciting oriented states (DCO ratios) [14,15] was adopted to determine  $\gamma$ -ray multipolarities and spins of the nuclear levels. For this purpose, a  $\gamma$ - $\gamma$  asymmetric matrix was created, where one axis corresponded to a  $\gamma$ -ray recorded by the detectors at 90°, whereas the other axis corresponded to the  $\gamma$ -ray recorded by the detectors at 40°. A gate corresponding to a  $\gamma$ -ray of known multipolarity was taken on one axis (say, the  $x$  axis) and the coincident spectrum was projected on the other axis. Next the same gate was set on the  $y$  axis and the projection was made along the  $x$  axis. Using gates of known quadrupole transitions, we define  $R_{\text{DCO}}$  as

$$R_{\text{DCO}} = \frac{I_{\gamma_1 \text{ at } 40^\circ, \text{ gated with } \gamma_2 \text{ at } 90^\circ}}{I_{\gamma_1 \text{ at } 90^\circ, \text{ gated with } \gamma_2 \text{ at } 40^\circ}}. \quad (1)$$

Usually the gate is chosen to set on a stretched quadrupole ( $E2$ ) transition, then theoretically  $R_{\text{DCO}} = 1.0$  is expected for stretched quadrupole transitions and  $R_{\text{DCO}} \approx 0.5$  for dipole transitions. Assuming stretched transitions, the intensities of the transitions that had the same multipolarity as the gated  $\gamma$ -ray were approximately the same in both spectra. For  $\gamma$ -rays of different multipolarities, the intensities differed by a factor of almost 2.

The clover detectors were utilized as Compton polarimeters to determine the electromagnetic character of the  $\gamma$ -rays [16–19]. The linear polarization of the radiation can typically be determined through the difference between the number of Compton scattered  $\gamma$ -rays in the reaction plane  $N_{\parallel}$  and the number in the reaction plane perpendicular to it,  $N_{\perp}$ . Two  $E_{\gamma}$ - $E_{\gamma}$  matrices were constructed; events were placed along one axis that contained the energy recorded in any one of the detectors, whereas the other axis corresponded to the energy scattered in a perpendicular or parallel segment of the clover detector with respect to the beam axis. From the projected spectra, the numbers of  $\gamma$ -rays with a scattering axis perpendicular ( $N_{\perp}$ ) and parallel ( $N_{\parallel}$ ) to the emission plane were obtained for a given  $\gamma$ -ray. From these spectra, the asymmetry parameter  $\Delta_{\text{IPDCO}}$  was obtained using the

relation

$$\Delta_{\text{IPDCO}} = \frac{a(E_{\gamma})N_{\perp} - N_{\parallel}}{a(E_{\gamma})N_{\perp} + N_{\parallel}}, \quad (2)$$

where  $N_{\perp}$  and  $N_{\parallel}$  are the intensities of the scattered photons perpendicular and parallel to the direction of the reaction plane, respectively. The parameter  $a$  denotes the correction owing to the asymmetry in response of the clover segments. This correction, defined as

$$a(E_{\gamma}) = \frac{N_{\parallel}(\text{unpolarized})}{N_{\perp}(\text{unpolarized})} \quad (3)$$

was determined as a function of  $\gamma$ -ray energy using  $\gamma$ -rays from a  $^{152}\text{Eu}$  radioactive source.

For the present setup, the energy dependence of the correction factor  $a$  was found to be as  $a(E_{\gamma}) = a_0 + a_1 E_{\gamma}$ , where,  $a_0 = 1.03$  and  $a_1 \sim 10^{-5}$ . This method of evaluating asymmetry is called the integrated polarization-directional correlation from oriented nuclei (IPDCO) [17–19]. This involves all the clover detectors placed in the reaction plane so that we may get the measurable polarization for weak transitions. Positive and negative values of  $\Delta_{\text{IPDCO}}$  correspond to stretched electric and magnetic transitions, respectively. A near-zero value is indicative of a possible admixture. As we use the data from the detectors at all angles in the reaction plane, we may not perform quantitative polarization measurements. However, we may obtain useful information about the nature of the  $\gamma$ -ray of interest. The polarization sensitivity is measured by measuring the asymmetry parameter ( $\Delta_{\text{IPDCO}}$ ) and verifying multipolarity for the well-known  $E2$  and  $M1$  transitions.

## III. RESULTS AND DISCUSSION

From the analysis of the  $\gamma$ - $\gamma$  matrix, intensities of transitions, DCO ratios, and proper gating, we established the level scheme of  $^{178}\text{Os}$ , as shown in Fig. 1. The bands are labeled 1–4 to facilitate discussion. Spins of the levels were determined from the  $R_{\text{DCO}}$  ratios and the parity assignments are based on polarization measurements. In addition to the transitions reported by Dracoulis *et al.* [9], 17 new transitions, that is, 144, 185, 271, 355, 398, 502, 532, 546, 562, 633, 750, 1200, 1513, 1563, 1576, 1589, and 1778 keV, were identified. These transitions are marked by asterisks in the level scheme (Fig. 1). A new additional side band (band 4) was also observed in the present work. Representative spectra, gated on transitions 132 and 144 keV, are shown in Figs. 2 and 3. These spectra are background subtracted and the negative counts are eliminated. The  $\gamma$ -rays identified with this nucleus are summarized in Table I according to their energies, relative intensities, spins, and parity and multipolarity assignments. Results of polarization measurements are shown in Fig. 4.

The levels of the ground-state band (band 1) up to the  $16^+$  state, band 1a up to  $24^+$ , and band 1b up to  $22^+$  are confirmed as reported by Dracoulis *et al.* [9]. We did not see the 834-keV transition ( $26^+ \rightarrow 24^+$ ) of band 1a as reported earlier by Dracoulis *et al.* in coincidence with the 643-, 719-, and 772-keV  $\gamma$  transitions. However, in the present data the 834-keV transition ( $24^+ \rightarrow 22^+$ ) was seen in coincidence with the 722-keV doublet  $\gamma$  transition of the yrare band (band 1b) in

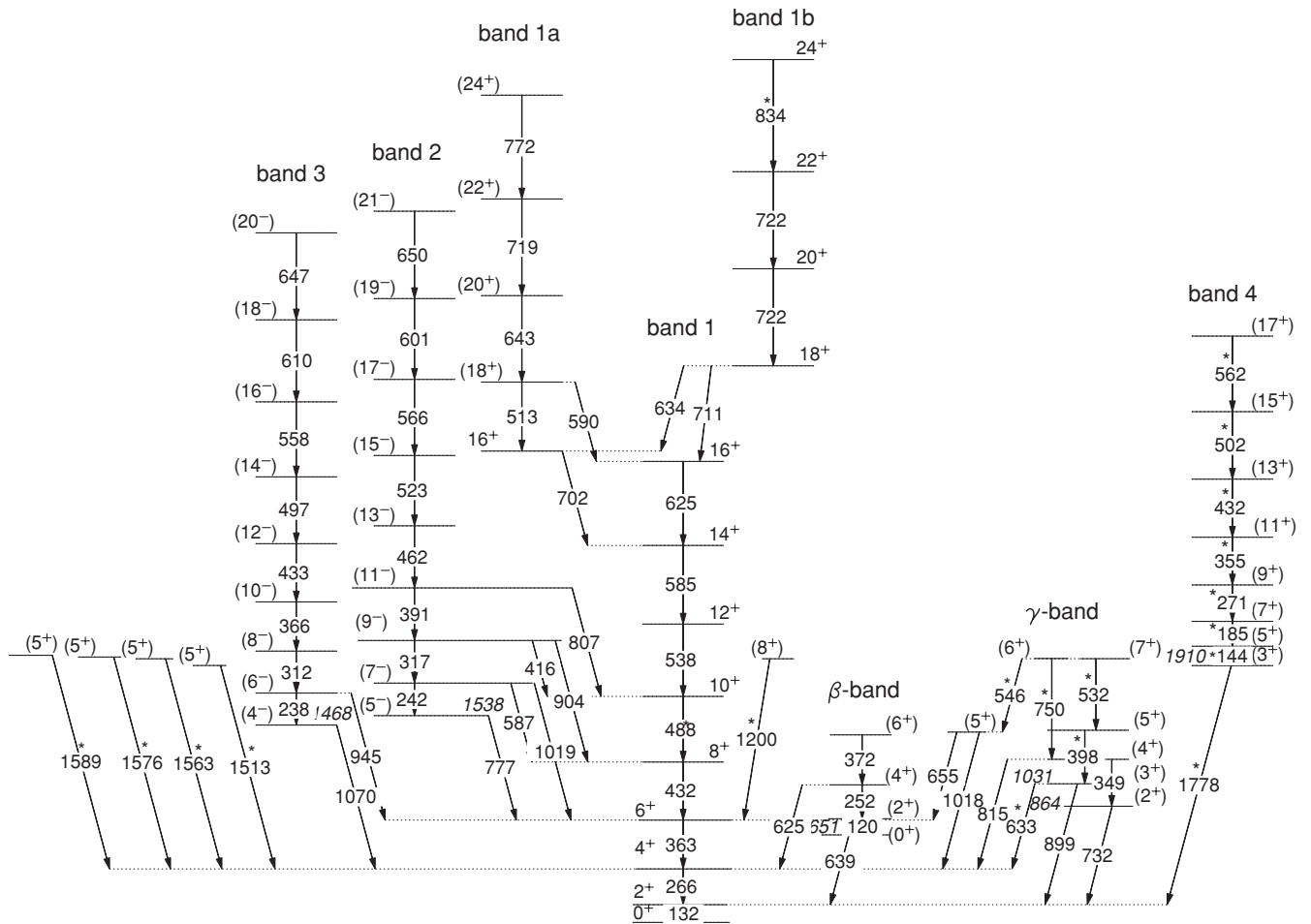


FIG. 1. Level scheme for  $^{178}\text{Os}$  populated in the  $^{165}\text{Ho}(^{20}\text{Ne}, p6n)^{178}\text{Os}$  reaction. Newly observed transitions are marked with an asterisk. Energies are marked within  $\pm 1$  keV. Spin and parity assignments, given in parentheses, are tentative.

place of the 743-keV transition tentatively placed at 1167 keV in this band by Dracoulis *et al.* [9]. A  $\beta$ -band, tentatively placed by Dracoulis *et al.*, was not observed in this study. However, the negative-parity bands (bands 2 and 3) assigned by Dracoulis *et al.* [9] were observed in this work.

The  $\beta$ - and  $\gamma$ -bands observed by Kibedi *et al.* [10] were observed by us, with the addition of a few new transitions. On the basis of the DCO and linear polarization analysis, the 398- and 532-keV intraband transitions in the  $\gamma$ -band and the 732-keV ( $2_2^+ \rightarrow 2_1^+$ ) and 815-keV ( $4_2^+ \rightarrow 4_1^+$ ) interband transitions from the  $\gamma$ -band to the ground-state band are assigned as electric quadrupole transitions. The interband transition of 899 keV ( $3^+ \rightarrow 2^+$ ) from the  $\gamma$ -band to the ground-state band is assigned as of  $M1/E2$  character from the present DCO and polarization measurements. The 252-keV ( $4_4^+ \rightarrow 2_2^+$ ) intraband transition of the  $\beta$ -band and the 639-keV ( $2_2^+ \rightarrow 2_1^+$ ) interband transition from the  $\beta$ -band to the ground-state band are assigned as electric quadrupole transitions.

We observed a number of single transitions without any band structure; for example, the 1200-keV transition ( $8^+ \rightarrow 6^+$ ) is assigned as  $E2$  on the basis of DCO and polarization measurements, whereas the 1513-, 1563-, 1576-, and 1589-keV transitions feeding to  $4^+$  are assigned as of dipole character on the basis of their DCO ratios.

A new side band (band 4) in the level scheme based on the band-head energy at 1910 keV was identified for the first time. This band exhibits a very complex decay pattern, with a single linking transition of 1778 keV to the  $2^+$  state of the ground-state band. A similar band was observed in  $^{180}\text{Os}$  produced by the  $6n$  channel in the  $^{150}\text{Nd}(^{36}\text{S}, 6n)$  reaction [20]. The PACE calculation for all nuclei populated in this reaction is shown in Fig. 5. Experimentally we also measured the excitation function for this nucleus from energies of 135 to 160 MeV and found that 150 MeV is the best energy for the population of this nucleus.

We identified the  $^{178}\text{Os}$  nucleus on the basis of the 132-keV transition ( $2^+ \rightarrow 0^+$ ) that is present only in this nucleus and not in any other  $^{177-179}\text{Ir}$  nuclei populated (Fig. 5) at this energy. This band is clearly visible in the spectrum (Fig. 3) gated with the 132-keV transition. Also, in reverse gating with the 144-keV transition belonging to this band (Fig. 3), the 132-keV transition is in coincidence with all the transitions of this band. Therefore, we are confident that this band belongs to the  $^{178}\text{Os}$  nucleus.

On the basis of the DCO value and polarization measurement, we adopted  $M1$  multipolarity for the 1778-keV transition, therefore band 4 is assigned positive parity. On the basis of the DCO ratio, the interband transitions in the

TABLE I. Excitation energies (keV), initial and final spins for transitions,  $\gamma$ -ray energies (keV), relative intensities, DCO ratios, and multiplicities of transitions belonging to the  $^{178}\text{Os}$  nucleus.

$E_i$	$J_i^\pi \rightarrow J_f^\pi$	$E_\gamma$	$I_\gamma^a$	$R_{\text{DCO}}$	Multiplicity
132	$2^+ \rightarrow 0^+$	132	100	1.0(0.016) <sup>b</sup>	$E2$
2054	$5^+ \rightarrow 2^+$	144	7.0	1.2(0.031) <sup>c</sup>	$E2$
2239	$7^+ \rightarrow 5^+$	185	6.4	1.1(0.038) <sup>c</sup>	$E2$
1706	$6^- \rightarrow 4^-$	238			$E2$
1780	$7^- \rightarrow 5^-$	242	4.0		$E2$
1023	$4^+ \rightarrow 2^+$	252	1.6	0.98(0.022) <sup>c</sup>	$E2$
398	$4^+ \rightarrow 2^+$	266	>140	1.1(0.026) <sup>c</sup>	$E2$
2510	$(8^+) \rightarrow (6^+)$	271	9.5	1.12(0.028) <sup>c</sup>	$E2$
2018	$8^- \rightarrow 6^-$	311	2.0	1.23(0.08) <sup>b</sup>	$E2$
2097	$9^- \rightarrow 7^-$	317	5.3	1.32(0.06) <sup>b</sup>	$E2$
1213	$(4^+) \rightarrow (2^+)$	349			$(E2)$
2865	$(11^+) \rightarrow (9^+)$	355	1.9		$(E2)$
761	$6^+ \rightarrow 4^+$	363	55	1.1(0.012) <sup>b</sup>	$E2$
2384	$10^- \rightarrow 8^-$	366	4.8	0.97(0.049) <sup>b</sup>	$E2$
1395	$6^+ \rightarrow 4^+$	373	3.3		$E2$
2488	$11^- \rightarrow 9^-$	391	3.7	1.5(0.075) <sup>b</sup>	$E2$
1429	$5^+ \rightarrow 3^+$	398	3.6	1.3(0.080) <sup>b</sup>	$E2$
2097	$9^- \rightarrow 10^+$	416			$E1$
1193	$8^+ \rightarrow 6^+$	432	29.2	1.06(0.08) <sup>b</sup>	$E2$
3297	$(13^+) \rightarrow (11^+)$	432			$E2$
2817	$12^- \rightarrow 10^-$	433			$E2$
2950	$13^- \rightarrow 11^-$	462	2.3	1.1(0.052) <sup>b</sup>	$E2$
1681	$10^+ \rightarrow 8^+$	488	16.0	0.97(0.019) <sup>b</sup>	$E2$
3314	$14^- \rightarrow 12^-$	497	4.2	1.06(0.08) <sup>b</sup>	$E2$
3798	$15^+ \rightarrow 13^+$	501	1.5		$(E2)$
4019	$18^+ \rightarrow 16^+$	513	1.3		$E2$
3473	$15^- \rightarrow 13^-$	523	2.0	1.35(0.037) <sup>b</sup>	$E2$
1961	$(7^+) \rightarrow 5^+$	532	1.3	1.1(0.03) <sup>c</sup>	$E2$
2219	$12^+ \rightarrow 10^+$	538	11.2	1.07(0.025) <sup>b</sup>	$E2$
1962	$7^+ \rightarrow 5^+$	546	2.0	0.96(0.040) <sup>b</sup>	$E2$
3872	$16^- \rightarrow 14^-$	558	1.8	1.06(0.08) <sup>b</sup>	$E2$
4360	$(17^+) \rightarrow (15^+)$	562	0.87		$(E2)$
4039	$17^- \rightarrow 15^-$	566	4.3	0.98(0.050) <sup>b</sup>	$E2$
2804	$14^+ \rightarrow 12^+$	585	10.5	0.99(0.019) <sup>b</sup>	$E2$
1780	$7^- \rightarrow 8^+$	587			$E2$
4019	$18^+ \rightarrow 16^+$	590	1.5	1.14(0.028) <sup>b</sup>	$E2$
4640	$19^- \rightarrow 17^-$	601	2.0	1.2(0.032) <sup>b</sup>	$E2$
4482	$18^- \rightarrow 16^-$	610	1.1	1.1(0.048) <sup>b</sup>	$E2$
3429	$16^+ \rightarrow 14^+$	624	17.5	0.98(0.032) <sup>b</sup>	$E2$
1023	$4^+ \rightarrow 4^+$	625			$(E2)$
1031	$3^+ \rightarrow 4^+$	633			$E2$
4140	$18^+ \rightarrow 16^+$	634	4.0	1.23(0.035) <sup>b</sup>	$E2$
8216	$2^+ \rightarrow 2^+$	639	11.2	1.1(0.03) <sup>c</sup>	$E2$
4662	$20^+ \rightarrow 18^+$	643	1.2	1.3(0.049) <sup>d</sup>	$E2$
1416	$(5^+) \rightarrow 4^+$	655	2.0		$(M1/E2)$
5129	$20^- \rightarrow 18^-$	647	1.3	1.25(0.05) <sup>b</sup>	$E2$
5290	$21^- \rightarrow 19^-$	650	1.0		$E2$
3506	$16^+ \rightarrow 14^+$	702	6.0	1.15(0.065) <sup>d</sup>	$E2$
4140	$18^+ \rightarrow 16^+$	711	2.6	1.4(0.072) <sup>d</sup>	$E2$
5381	$(22^+) \rightarrow 20^+$	719			$E2$
4862	$(20^+) \rightarrow 18^+$	722	2.2	1.11(0.056) <sup>d</sup>	$E2$
864	$(2^+) \rightarrow 2^+$	732	5.8	1.13(0.045) <sup>c</sup>	$E2$
1963	$(6^+) \rightarrow 4^+$	750			$E2$
6153	$24^+ \rightarrow 22^+$	772	1.0		$E2$
1538	$5^- \rightarrow 6^+$	777	3.5	0.54(0.032) <sup>b</sup>	$E1$

TABLE I. (*Continued.*)

$E_i$	$J_i^\pi \rightarrow J_f^\pi$	$E_\gamma$	$I_\gamma^a$	$R_{\text{DCO}}$	Multiplicity
2488	$11^- \rightarrow 10^+$	807	0.9		$E1$
1213	$4^+ \rightarrow 4^+$	815	4.5	1.1(0.03) <sup>b</sup>	$E2$
6418	$24^+ \rightarrow 22^+$	834	1.7		$E2$
1031	$3^+ \rightarrow 2^+$	899	12	0.64(0.06) <sup>c</sup>	$M1/E2$
2097	$9^- \rightarrow 8^+$	904	1.8	0.46(0.029) <sup>d</sup>	$E1$
1706	$6^- \rightarrow 6^+$	945	2.8	0.47(0.026) <sup>b</sup>	$E1$
1416	$(5^+) \rightarrow 4^+$	1018	7.0	0.59(0.020) <sup>b</sup>	$M1/E2$
1780	$7^- \rightarrow 6^+$	1019			$E1$
1468	$4^- \rightarrow 4^+$	1070	0.84	0.45(0.032) <sup>b</sup>	$E1$
1213	$4^+ \rightarrow 2^+$	1080	3.2	1.1(0.050) <sup>c</sup>	$E2$
1961	$8^+ \rightarrow 6^+$	1200	10.2	1.13(0.07) <sup>d</sup>	$E2$
1911	$(5^+) \rightarrow 4^+$	1513	1.8	0.75(0.047) <sup>b</sup>	$(M1/E2)$
1961	$(5^+) \rightarrow 4^+$	1563	1.9	0.70(0.039) <sup>b</sup>	$(M1/E2)$
1974	$(5^+) \rightarrow 4^+$	1576	2.2	0.68(0.043) <sup>b</sup>	$(M1/E2)$
1987	$(5^+) \rightarrow 4^+$	1589	2.3	0.78(0.045) <sup>b</sup>	$(M1/E2)$
1910	$(3^+) \rightarrow 2^+$	1778	6.0	0.64(0.047) <sup>c</sup>	$(M1/E2)$

<sup>a</sup>Errors in relative intensities are estimated to be less than 5% of the quoted values for strong transitions ( $I_\gamma \geq 10$ ) and less than 20% for weaker transitions ( $I_\gamma < 10$ ). Values are normalized to 100% for the 132-keV transition of the ground-state band.

<sup>b</sup> $R_{\text{DCO}}$  ratio from the gate on the 266-keV quadrupole transition.

<sup>c</sup> $R_{\text{DCO}}$  ratio from the gate on the 132-keV quadrupole transition.

<sup>d</sup> $R_{\text{DCO}}$  ratio from the gate on the 363-keV quadrupole transition.

new band, for example, 144 keV ( $5^+ \rightarrow 3^+$ ), 185 keV ( $7^+ \rightarrow 5^+$ ), and 271 keV ( $9^+ \rightarrow 7^+$ ), are assigned as quadrupole transitions.

### A. Microscopic Hartree-Fock calculation with angular momentum projection

The experimental results were studied with deformed Hartree-Fock (HF) and angular momentum ( $J$ ) projection [21,22]. The deformed HF equation is derived from the nuclear Hamiltonian, which consists of the single-particle and the residual two-body interaction terms:

$$H = \epsilon + V. \quad (4)$$

Here  $\epsilon$  stands for single-particle energies of spherical-shell-model orbits and  $V$  stands for  $pp, pn$ , and  $nn$  two-body residual interactions. Prolate HF calculations for valence nucleons lying outside the  $^{132}\text{Sn}$  core were performed for the  $^{178}\text{Os}$  nucleus, using the surface- $\delta$  residual interaction [23,24] (with strength 0.3 MeV for  $pp, pn$ , and  $nn$  interactions) within a model space of one major shell each for protons and neutrons. We used spherical Nilsson single-particle energies [25]. The  $3s_{1/2}, 2d_{3/2}, 2d_{5/2}, 1g_{7/2}, 1h_{11/2}$ , and  $1h_{9/2}$  proton states have energies of 3.654, 3.288, 0.731, 0.0, 1.705, and 7.1 MeV, and the  $3p_{1/2}, 3p_{3/2}, 2f_{5/2}, 2f_{7/2}, 1h_{9/2}$ , and  $1i_{13/2}$  neutron states have energies of 4.462, 2.974, 3.432, 0.0, 0.686, and 1.487 MeV, respectively.

Prolate HF orbits for  $^{178}\text{Os}$  are shown in Fig. 6. The HF orbits shown are doubly degenerate and are labeled by the  $m$  quantum numbers, the sum total of which, for the occupied orbits, gives the  $K$  value. The HF orbits provide a realistic deformed intrinsic structure for study of the high spin band

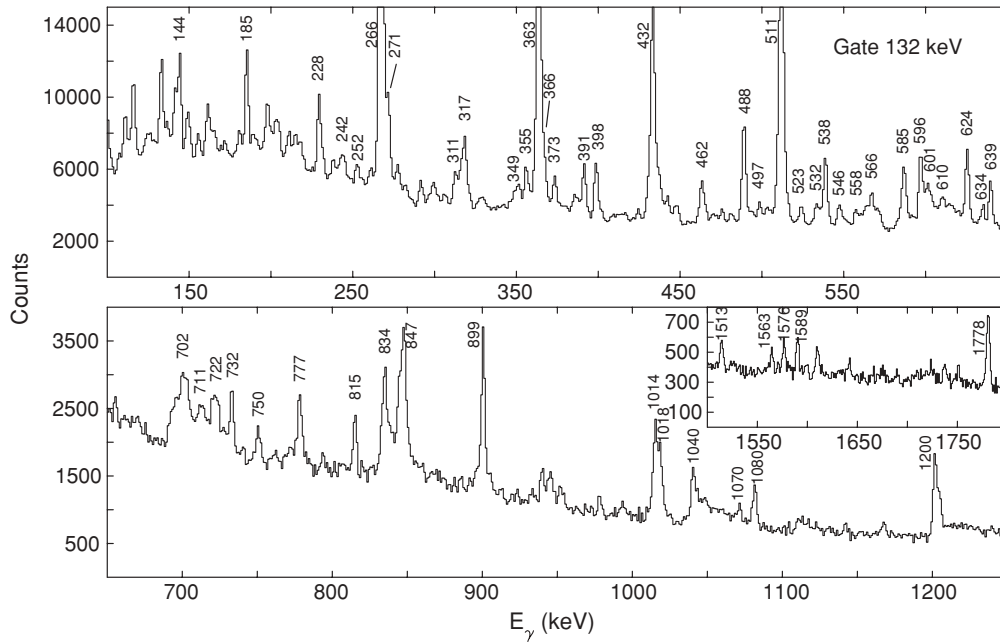


FIG. 2.  $\gamma$ - $\gamma$  coincidence spectrum with the gate on the 132-keV transition.

structure. Angular momentum projection for the  $K = 0^+$   $(1/2^-)^{2n}$  configuration and excitation based on it reproduce the observed ground-state band 1 as shown in Fig. 7. Because  $1/2^-$  is prolate-like,  $K = 0^+$  with  $(1/2^-)^{2n}$  forms the ground-state band with prolate deformation. The Fermi level lies between the  $7/2^-$  and the  $1/2^-$  orbits, which are almost degenerate. The  $K = 0^+$  band is also formed with the last two neutrons in the  $m = 7/2^-$  oblate orbit, which lies a little higher in energy as shown in Fig. 7. At  $I = 16\hbar$  two side bands appear in the experimental spectra. The degeneracy of the two negative-parity orbits (the oblate driving with  $m = 7/2^-$  and prolate driving with  $m = 1/2^-$ ) greatly influences the band structure in this nucleus and the splitting of band 1 into 1a and 1b at higher excitation energies may be for this reason.

For the negative-parity state the excitation of the neutron from the  $1/2^-$  state to the nearby  $7/2^+$  state favors a  $K = 4^-$  band, which is observed in our experimental data at 1468 keV as shown in Fig. 1. The  $K = 5^-$  band, which starts at 1538 keV, is probably formed owing to the excitation of one neutron from the  $1/2^-$  to the nearby  $9/2^+$  state (Fig. 6).

**B. Alignment behavior of bands in  $^{178}\text{Os}$**

Additional important properties of the bands can be obtained by examining the experimental Routhian and aligned angular momentum. Experimental Routhians and aligned angular momenta extracted for different bands are shown

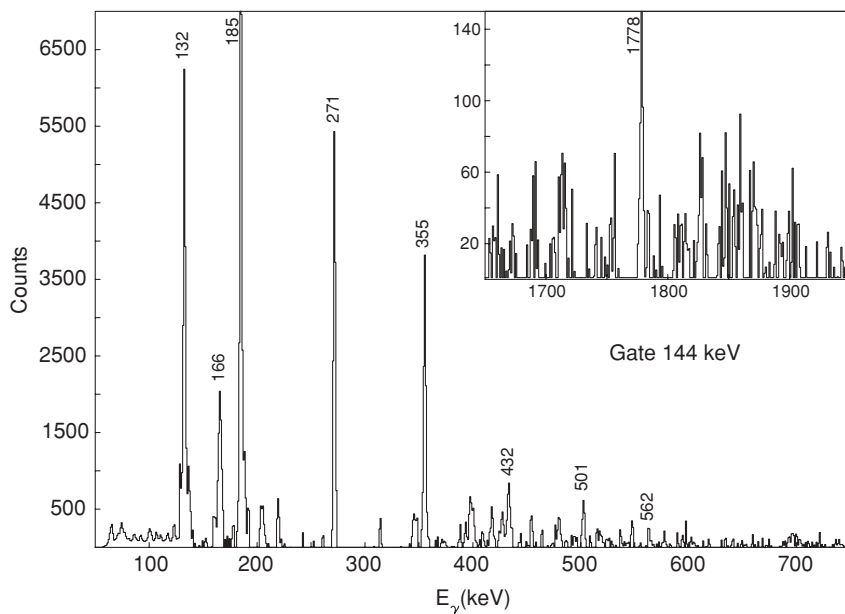


FIG. 3.  $\gamma$ - $\gamma$  coincidence spectrum with the gate on the 144-keV transition.

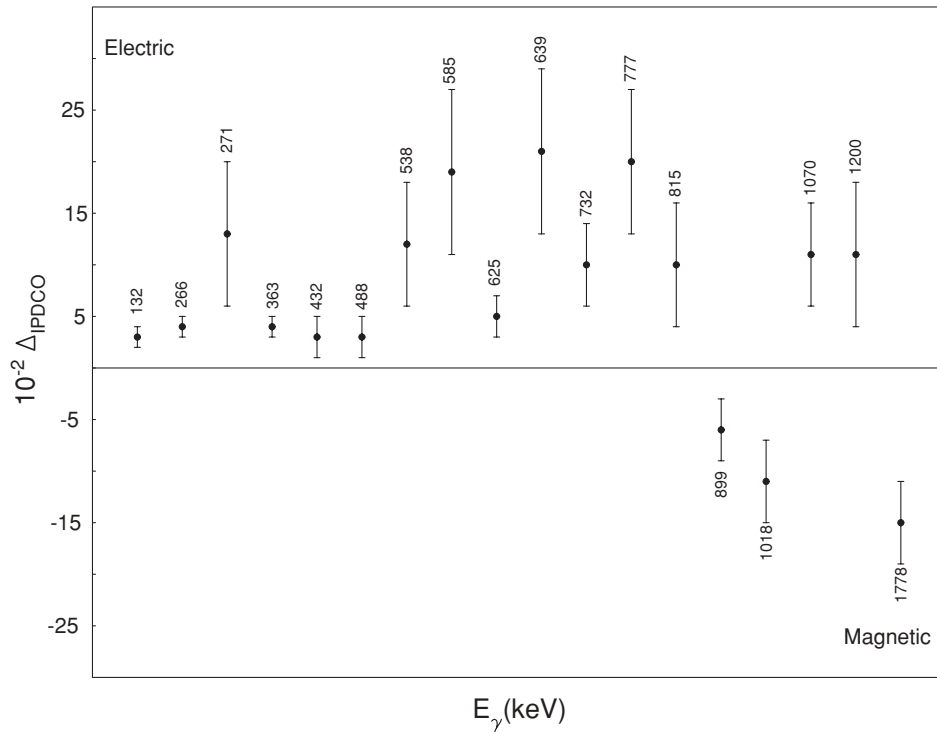


FIG. 4. Experimental  $\gamma$ -ray asymmetry parameter  $\Delta_{IPDCO}$ , from polarization measurements plotted for  $\gamma$ -ray transitions of  $^{178}\text{Os}$ . A positive value corresponds to an electric transition and a negative value indicates a magnetic transition. Quoted errors are from peak fitting and background subtraction.

in Figs. 8 and 9, respectively, as a function of rotational frequency using Harris parameters [26], as  $J_0 = 25\hbar^2 \text{MeV}^{-1}$  and  $J_1 = 60\hbar^4 \text{MeV}^{-3}$ . They were deduced from the excitation energies  $E$  and spins  $I$  of the observed levels and were obtained by subtracting the energy and angular momentum of the collective rotation. As shown in Fig. 9 band 1a shows the first band crossing at a rotational frequency of  $\hbar\omega = 0.31 \text{MeV}$ , which is somewhat higher than the frequency of  $0.24 \text{MeV}$  predicted by Bengtsson *et al.* [27]. The theoretical proton and neutron Routhians have been plotted for the even- $A$  ( $^{178-180}\text{Os}$ ) isotopes in Ref. [27]. They have an initial alignment of  $8.5\hbar$  as shown in Fig. 9 and are caused due to the rotation alignment

of an  $i_{13/2}$  quasineutron pair. A similar trend was observed by Lieder *et al.* [20] in  $^{180}\text{Os}$ . The band crossing is associated with a deformation change from  $\beta_2 = 0.24$ ,  $\beta_4 = 0.025$ , and  $\gamma = -1^\circ$  for the ground band to  $\beta_2 = 0.21$ ,  $\beta_4 = 0.045$ , and  $\gamma = -12^\circ$  for the crossing band of  $(\nu i_{13/2})^2$  configuration according to the calculations of Wyss *et al.* [28]. A similar trend was predicted by our total Routhian surface (TRS) calculations, performed within the Woods-Saxon cranking formalism [29,30]. For these calculations the average mean field is taken to be a rotating Woods-Saxon potential [31,32] with a monopole type of pairing interaction. TRS results are plotted in Fig. 10 for the frequencies  $\hbar\omega = 0.0 \text{MeV}$  and

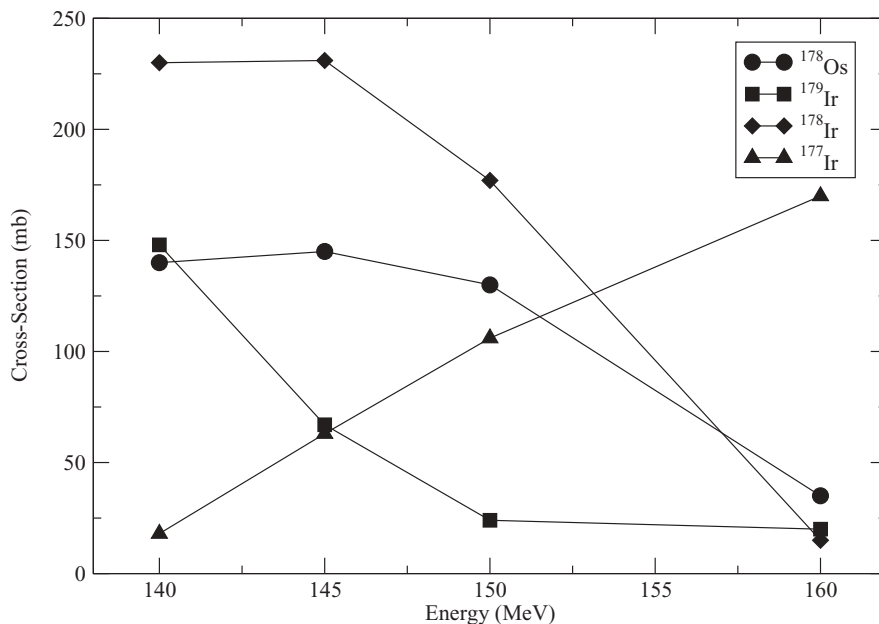


FIG. 5. PACE calculations showing variation of the reaction cross section with beam energy for the reaction used in the present work.

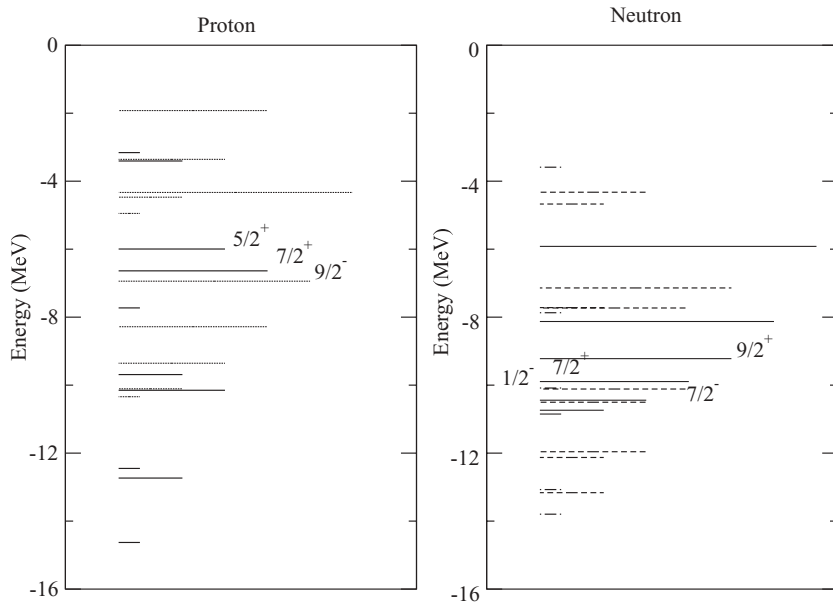


FIG. 6. Prolate HF orbits of  $^{178}\text{Os}$ . The Fermi level of the neutron is between  $1/2^-$  and  $7/2^-$ , and that of the proton is between  $9/2^-$  and  $7/2^+$ .

$\hbar\omega = 0.22$  MeV, respectively. The TRS plot shows a minimum at ( $\hbar\omega = 0.0$ ) with  $\beta_2 = 0.21$  and  $\gamma = 0^\circ$  in Fig. 10(a), and this minimum is shifted toward  $\beta_2 = 0.19$  and  $\gamma = -15^\circ$  at a rotational frequency of  $\hbar\omega = 0.22$  MeV as shown in Fig. 10(b). This indicates that the nucleus is prolate deformed with  $\beta_2 = 0.209(7)$ , as also predicted by lifetime measurement [33] of the 132-keV  $2^+$  state in the ground state and has a tendency toward  $\gamma$  vibration at higher excitation, which gives rise to the  $\gamma$ -band. The triaxial model was introduced by Davydov and Filippov [34] for triaxially deformed nuclei and was further extended in the form of the coupled rotation-vibration model [35,36]. In this model an axially symmetric ground state is assumed ( $\beta = \beta_0, \gamma = \gamma_0$ ) and the potential is expanded around this minimum in the fixed-body system, introducing a small deviation in  $\beta$  and  $\gamma$  degrees of freedom as

$$V(\beta, \gamma) = \frac{1}{2}C(\beta - \beta_0)^2 + D\gamma^2, \quad (5)$$

where  $C$  and  $D$  are constants for a nucleus. This model is extremely successful in explaining the structure of the rotational nuclei in the framework of coupling of  $\beta$  and/or  $\gamma$  vibrations with rotation about the symmetry axis, resulting in the  $\beta$ - and/or  $\gamma$ -vibrational bands. The value of  $\gamma$  calculated from the energies of the  $2_1^+$  and  $2_2^+$  states using the asymmetric rotor model [34],

$$\frac{E_2(2)}{E_1(2)} = \frac{[1 + \sqrt{1 - \frac{8}{9}\sin^2(3\gamma)}]}{[1 - \sqrt{1 - \frac{8}{9}\sin^2(3\gamma)}]} = \frac{864}{132}, \quad (6)$$

also predicts  $\gamma = 15^\circ$ , which is close to the value indicated by TRS calculation. The higher  $6^+$  in the  $\gamma$ -band may be perturbed owing to the rotational coupling or owing to the interaction of the intruder orbits.

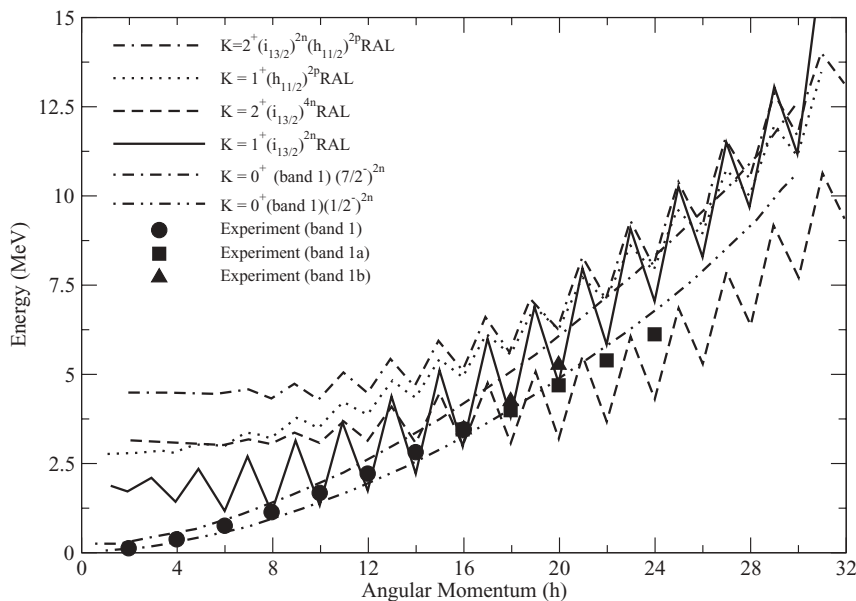


FIG. 7. Comparison of experimental levels in positive-parity bands with results of the microscopic deformed Hartree-Fock model.

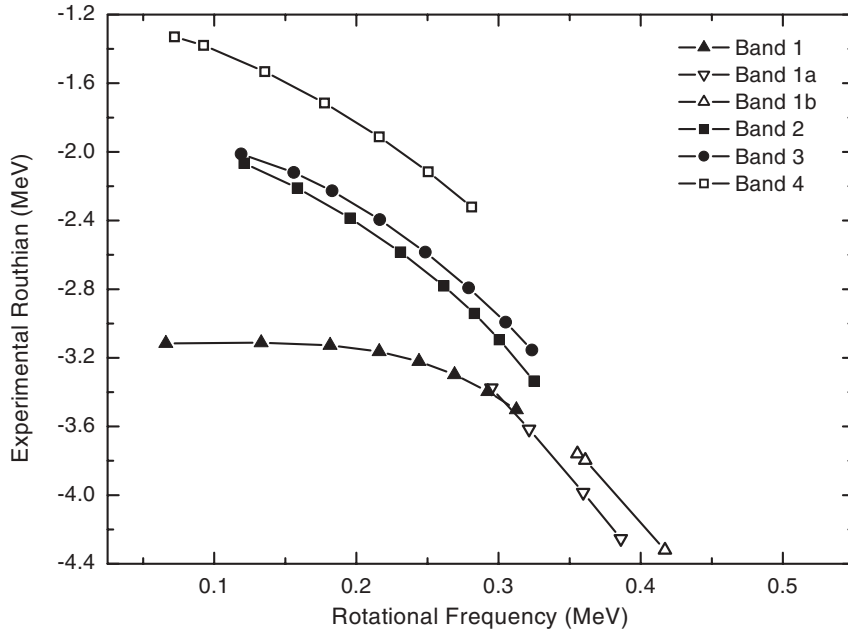


FIG. 8. Experimental Routhian plots for the bands in  $^{178}\text{Os}$  using  $J_0 = 25\hbar^2 \text{MeV}^{-1}$  and  $J_1 = 60\hbar^4 \text{MeV}^{-3}$  as reference core parameters.

Band 1b starts with an initial alignment of  $\approx 6\hbar$  at  $\hbar\omega = 0.36 \text{ MeV}$  and increases to a value of  $\approx 10\hbar$  at a rotational frequency of  $\hbar\omega = 0.37 \text{ MeV}$ . Band 1b seems to be the continuation of the ground-state band (band 1), which crosses band 1a at  $0.37 \text{ MeV}$ . The experimental Routhian plots show that above  $\hbar\omega = 0.35 \text{ MeV}$ , band 1b is approximately parallel to band 1a, as expected for the BC band from theoretical calculations [27]. The negative-parity bands (bands 2 and 3) have relatively large aligned angular momenta and display a similar frequency dependence of the aligned angular momentum. Both bands show a crossing in the frequency range  $0.15 \leq \hbar\omega \leq 0.25 \text{ MeV}$  with an alignment gain of  $\approx 3\hbar$ , corresponding to an alignment of an  $i_{13/2}$  quasineutron pair. The new band, 4,

starts with an aligned angular momentum of  $1.8\hbar$  and shows no alignment till the angular momentum of  $6\hbar$ . This band may have a configuration similar to that of the  $(+, 1)_7$  band in  $^{180}\text{Os}$  formed by the  $6n$  reaction [20].

#### IV. SUMMARY

The level structure of the even-even  $^{178}\text{Os}$  nucleus has been studied with the six-clover-detector array using the heavy ion fusion evaporation reaction. Several new transitions belonging to this nucleus have been identified and a new side band has been observed. The level scheme has been substantially

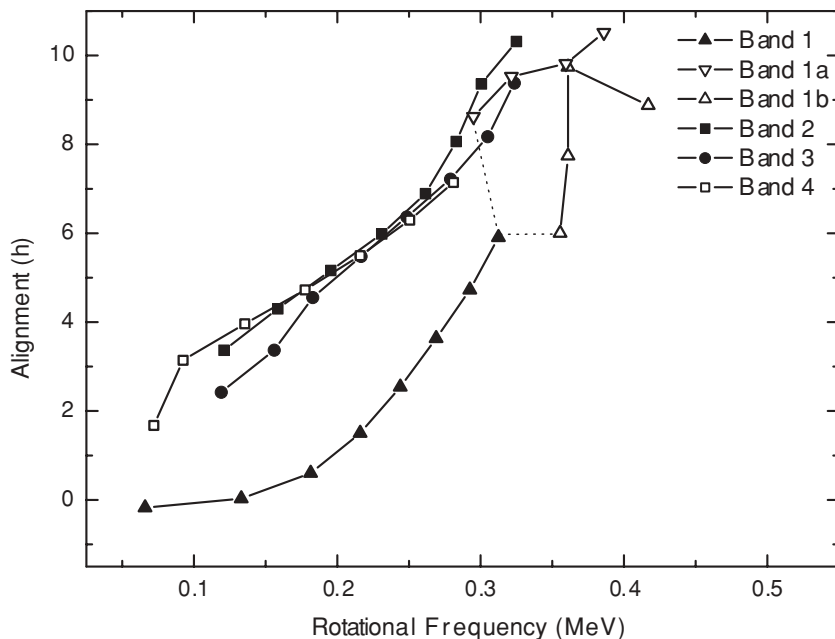


FIG. 9. Experimental alignment plots for the bands in  $^{178}\text{Os}$  using  $J_0 = 25\hbar^2 \text{MeV}^{-1}$  and  $J_1 = 60\hbar^4 \text{MeV}^{-3}$  as reference core parameters.

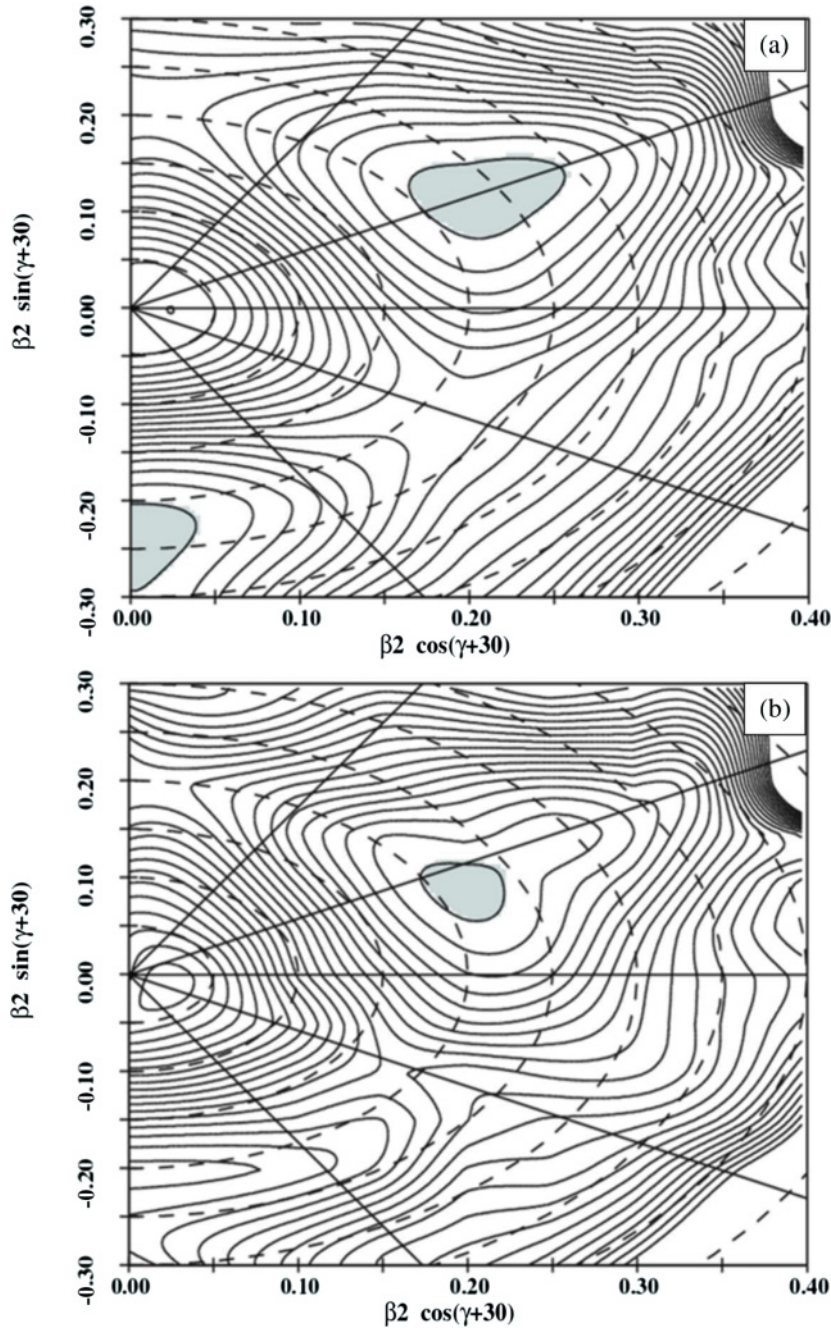


FIG. 10. (Color online) Total Routhian surface plots in the  $\beta_2$ - $\gamma$  plane for the positive-parity band in  $^{178}\text{Os}$  for rotational frequencies  $\hbar\omega = 0.0\text{ MeV}$  (a) and  $\hbar\omega = 0.22\text{ MeV}$  (b).

enhanced and a number of ambiguities in level structure reported earlier have been resolved. Experimental results are compared with the projected angular momentum deformed HF model calculations and cranked Woods-Saxon model calculations. This nucleus is found to be prolate deformed in the ground state but it has a tendency toward  $\gamma$ -softness at higher excitation as revealed by the cranked Woods-Saxon model and the geometric coupled rotation-vibration model.

#### ACKNOWLEDGMENTS

The authors would like to thank the accelerator crew for providing an excellent beam at the Variable Energy Cyclotron Centre, Calcutta. We also thank Dr. G. de Angelis and Professor Umesh Garg for discussion and provision of useful suggestions about the present work. Financial support from the UGC, IUC-DAEF, and CSIR is gratefully acknowledged.

- [1] J. D. Garrett and S. Frauendorf, Phys. Lett. **B108**, 77 (1982).  
 [2] A. Neskakis *et al.*, Phys. Lett. **B118**, 49 (1982).

- [3] W. F. Davison *et al.*, Z. Phys. **264**, 235 (1973).  
 [4] R. A. Warner, F. M. Bernthal, J. S. Boyno, T. L. Khoo, and G. Sletten, Phys. Rev. Lett. **31**, 835 (1973).

- [5] I. Ragnarsson, A. Sobieczewski, R. K. Sheline, S. E. Larsson, and B. Nerlo-Pomorska, *Nucl. Phys.* **A233**, 329 (1974).
- [6] R. M. Lieder *et al.*, *Proceedings of Symposium on Electromagnetic Properties of High Spin States*, Stockholm, Sweden (1985).
- [7] R. M. Lieder, G. Sletten, J. Borggreen, and J. Pedersen, *Nucl. Phys.* **A375**, 291 (1982).
- [8] G. D. Dracoulis, C. Fahlander, and M. P. Fewell, *Phys. Rev. Lett.* **45**, 1831 (1980).
- [9] G. D. Dracoulis, C. Fahlander, and M. P. Fewell, *Nucl. Phys.* **A383**, 119 (1982).
- [10] T. Kibedi, G. D. Dracoulis, A. P. Byrne, and P. M. Davison, *Nucl. Phys.* **A567**, 183 (1994).
- [11] J. Burde *et al.*, *Phys. Rev. C* **38**, R2470 (1988).
- [12] D. C. Radford, *Nucl. Instrum. Methods Phys. Res. A* **361**, 297 (1995).
- [13] N. S. Pattabiraman, S. N. Chintalapudi, and S. S. Ghugre, *Nucl. Instrum. Methods Phys. Res. A* **526**, 432 (2004).
- [14] F. S. Stephens, M. A. Deleplanque, R. M. Diamond, A. O. Macchiavelli, and J. E. Draper, *Phys. Rev. Lett.* **54**, 2584 (1985).
- [15] C. W. Beausang *et al.*, *Nucl. Instrum. Methods Phys. Res. A* **364**, 560 (1995).
- [16] G. Duchêne *et al.*, *Nucl. Instrum. Methods Phys. Res. A* **432**, 90 (1999).
- [17] K. Starosta, *Nucl. Instrum. Methods Phys. Res. A* **423**, 16 (1999).
- [18] Ch. Droste, *Nucl. Instrum. Methods Phys. Res. A* **430**, 260 (1999).
- [19] N. S. Pattabiraman *et al.*, *Phys. Rev. C* **65**, 044324 (2002).
- [20] R. M. Lieder *et al.*, *Nucl. Phys.* **A645**, 465 (1999).
- [21] G. Ripka, in *Advances in Nuclear Physics*, edited by M. Baranger and E. Vogt (Plenum Press, New York, 1968), Vol. 1, p. 183; D. M. Brink, in *Proceedings of the International School of Physics Course 36*, edited by C. Bloch (Academic Press, 1966), p. 247; M. R. Gunye and C. S. Warke, *Phys. Rev.* **156**, 1087 (1967).
- [22] Z. Naik and C. R. Prahara, *Phys. Rev. C* **67**, 054318 (2003).
- [23] A. Faessler, P. Plastino, and S. A. Moszkowski, *Phys. Rev.* **156**, 1064 (1967).
- [24] P. J. Brussard and P. W. M. Glaudemans, *Shell Model Applications in Nuclear Spectroscopy* (North-Holland, Amsterdam, 1977).
- [25] C. Gustafson, I. L. Lamm, B. Nilsson, and S. G. Nilsson, *Ark. Fysik.* **36**, 613 (1967).
- [26] S. M. Harris, *Phys. Rev.* **138**, B509 (1965).
- [27] R. Bengtsson, S. Frauendorf, and F. R. May, *At. Data Nucl. Data Tables* **35**, 15 (1986).
- [28] R. Wyss, W. Satula, W. Nazarewicz, and A. Johnson, *Nucl. Phys.* **A511**, 324 (1990).
- [29] P. Ring and P. Schuck, *The Nuclear Many Body Problems* (Springer-Verlag, Berlin, 1980), p. 244.
- [30] W. Nazarewicz, M. A. Riley, and J. D. Garrett, *Nucl. Phys.* **A512**, 61 (1990).
- [31] T. R. Werner and J. Dudek, *At. Data Nucl. Data Tables* **59**, 1 (1995).
- [32] T. R. Werner and J. Dudek, *At. Data Nucl. Data Tables* **50**, 179 (1992).
- [33] O. Moller, P. Petkov, B. Melon, A. Dewald, A. Fitzler, J. Jolie, D. Tonev, S. Christen, B. Saha, K. O. Zell, and M. Heidemann, *Phys. Rev. C* **72**, 034306 (2005).
- [34] A. S. Davydov and G. F. Filippov, *Nucl. Phys.* **8**, 237 (1958).
- [35] A. Faessler *et al.*, *Nucl. Phys.* **70**, 33 (1965).
- [36] J. Eisenberg and W. Greiner, *Nuclear Theory and Collective Models*, 3rd ed. (North-Holland, Amsterdam, 1972).